Khan, Y.; Marin, M.; Karinen, Reetta; Lehtonen, Juha; Kanervo, Jaana

1-Butanol dehydration in microchannel reactor: Kinetics and reactor modelling

Published in:
Chemical Engineering Science

DOI:
10.1016/j.ces.2015.07.026

Published: 01/01/2015

Document Version
Peer-reviewed accepted author manuscript, also known as Final accepted manuscript or Post-print

1-Butanol dehydration in microchannel reactor: Kinetics and reactor modelling

Yaseen Khan*, Minna Marin, Reetta Karinen, Juha Lehtonen, Jaana Kanervo

Department of Biotechnology and Chemical Technology, Aalto University School of Chemical Technology, P.O. Box 16100, 00076 Aalto, Finland.

Abstract

A structured microchannel reactor (MCR) coated with pure γ-Al_2O_3 was applied to investigate 1-butanol dehydration under atmospheric and isothermal conditions. Kinetic experiments were carried out and the advantages related to mass transfer properties with the application of MCR were explored under different reaction parameters and conditions. It was revealed that with the average coating thickness of 25 μm, the operation was free of diffusional limitations and hence intrinsic kinetics could be determined by describing the reactor as pseudohomogeneous PFR with reaction kinetic expressions incorporated. Experimental data was regressed using power-law kinetics with a simplified reaction scheme for 1-butanol dehydration to butenes and dibutylether as well as with mechanistic model involving surface butoxies as relevant species. Both models were able to describe the experimental observations and the estimated values for kinetic parameters were in physically meaningful order of magnitude. A dynamic mathematical model was developed including diffusional mass transport of components and reaction inside coating, whereas, in free channel, plug flow mass transport was considered. The proposed model besides reproducing the experimental results was also able to predict presence of diffusional limitations when coating thickness is increased beyond 40 μm. Furthermore, the simulation results show that for specific operation regimes Microchannel Reactor (MCR) outperforms packed-bed reactor, as mass transfer limitations can be appreciably reduced for 1-butanol dehydration.

Keywords:
1-Butanol, Dehydration, Microreactor, Kinetics, Modelling, Alumina

1. Introduction

1-Butanol, the four-carbon linear alcohol is considered one of the future bio-compounds for fuel and chemical use. So called biobutanol (1-butanol) produced from renewable sources by ABE fermentation process (Acetone, Butanol, Ethanol). Although the production of biobutanol is unfeasible yet compared to traditional production from crude oil, improving the process e.g. by means of metabolic engineering of the bacteria or by lowering the expenses of the needed separation processes, are widely researched. (Chen et al., 2014) Dehydration reactions of different primary and secondary alcohols have been studied and modeled in microchannel reactors, e.g. (Rouge et al., 2001; Hu et al., 2005; Chen et al., 2007), but 1-butanol dehydration reaction, to our knowledge has not been studied in a microchannel reactor. Dehydration of 1-butanol has been studied by applying different catalysts and reactor systems, and main products are reported as butene, dibutyl ether, water and butene isomers, such as, cis-2-butene, trans-2-butene and iso-butene (Knözinger and Köhne, 1966; Berteau and Delmon, 1989; Berteau et al., 1991; Hsu et al., 2009; West et al., 2009; Macho et al., 2001; Bernal and Trillo, 1980; Zhang et al., 2010; Giniestra et al., 1987; Mostafa and Youssef, 1998; Makarova, 1994; Chakor-Alami et al., 1984; Krampera and Beránek, 1986; West et al., 2009; Bautista, 1995; Delsarte and Grange, 2004).

1-Butanol dehydration reaction on γ-Al_2O_3 produces butenes, water, dibutyl ether and butene isomers as the main products. The reaction has also been studied as a test reaction for acidic sites of the catalyst: the product distribution especially the ratio between butene isomers is reported to depend on the acidity and the nature of the acidic sites of the catalyst (Berteau et al., 1991; Macias et al., 2006). The crystal structure of γ-Al_2O_3 and type of active sites are still reported to be a matter of discussion, due to defective non-stoichiometric spinel structure and shifting bands for hydroxyl groups

*Corresponding author.

(Busca, 2014; Phung et al., 2014). Recent spectroscopic data and most recent theoretical calculations about surface sites on γ-Al_2O_3 are summarized by research group of G. Busca. Besides other observations these authors have also reported from IR spectroscopic observations that γ-Al_2O_3 contains Lewis acid/base sites and surface hydroxyl groups. Phung et al. (2014) studied ethanol dehydration on different alumina samples and proposed a surface reaction mechanism in which ethoxy groups formed through surface hydroxyl groups and Lewis acid-base pairs, are proposed to be intermediate species for both diethyl ether and ethylene production. These recent spectroscopic findings and theoretical calculations provide an opportunity to test such mechanistic models, along with engineering type models (power law type kinetics), for other alcohol molecules as well, such as 1-butanol.

We acknowledge the contribution of recent spectroscopic studies (Busca, 2014; Phung et al., 2014) in developing further understanding of dehydration surface reaction mechanism of ethanol on γ-Al_2O_3. The proposed scheme by Phung et al. (2014), is generalized here for kinetic description for alcohol dehydration on γ-Al_2O_3. Under this scheme it is considered that alkoxy species serve as the intermediate species for the formation of olefins and ethers. These alkoxy species may be formed by two pathways (Figure 1), first: by attack of Lewis acid-base pairs on likely dissociative adsorbed alcohol with new OHs. Second: adsorption of alcohol on surface OH groups and releasing water.

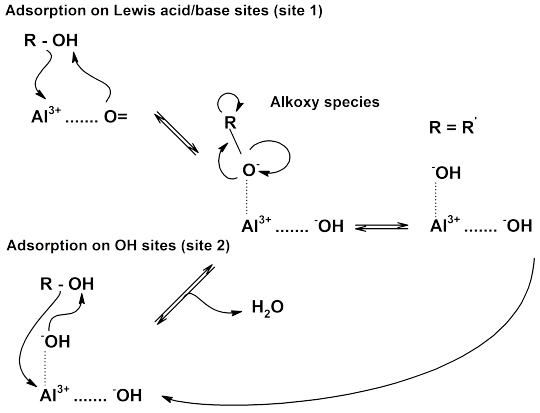

Figure 1 Adsorption reaction scheme for alkene formation, adapted from Phung et al. (2014).

For ether formation two pathways are considered. In first pathway (Figure 2), ether formation occurs by nucleophilic substitution reaction by attack of alkoxy group to H-bonded adsorbed undissociated alcohol, as proposed by Phung et al. (2014).

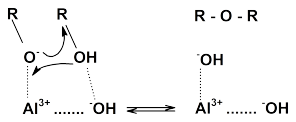

Figure 2 Surface reaction scheme I for ether formation, adapted from Phung et al. (2014).

The second pathway is assumed to be a dual site mechanism (Figure 3). In literature some studies for alcohol dehydration Berteau et al. (1985) and Decanio et al. (1992) have advocated this dual site mechanism. In general two neighboring alkoxy species formed through Lewis acid-base and basic sites on alumina, undergo a nucleophilic attack of the Lewis acid-base alkoxide species on positively polarized carbon in basic alkoxide species.

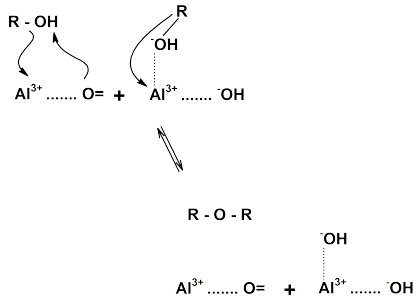

Figure 3 Surface reaction scheme II for ether formation, adapted from Berteau et al. (1985) and Decanio et al. (1992).

Microreactors are miniaturized reactor systems with at least one dimension below the submillimeter scale. Microchannel reactors consist of one or multiple parallel channels. In general, microchannel reactors are known for their good heat and mass transfer properties enabling nearly isothermal operation of highly exothermic or endothermic reactions (Walter et al., 2005). However, in catalytic microchannel reactors, where the channel walls are coated with the catalyst, both internal and external mass transport limitations need to be considered. External and internal mass transport considerations have been discussed by e.g. Kolb and Hessel (2004), Görke et al. (2009) and Lopes et al. (2011), who have applied modified forms of Mears criterion (Mears, 1971) and Weisz-Prater criterion (Weisz and Prater, 1954), for wall coated microchannel reactors. The thickness of the catalyst coating is the most signif-

icant parameter determining whether the internal mass transfer can be neglected (Reschetilowski, 2013).

Different approaches have been reported in literature, e.g. by Spatenka et al. (2005), Walter et al. (2005), Görke et al. (2009) and Schmidt et al. (2013), to model coated microchannel reactors for gas-phase reactions. In all these cases, plug flow model was applied to determine kinetic parameters. In addition to kinetic studies, Spatenka et al. (2005) and Walter et al. (2005) also developed a 2D dynamic model to simulate the coated microchannel reactor. Spatenka et al. (2005) modeled cylindrical channel in 2D considering axial convection and axial dispersion in an empty space with the external mass transfer coefficient. In the solid phase, internal diffusion and reaction inside the catalyst layer were considered. Walter et al. (2005) modeled the cylindrical channel in 2D considering axial convection, dispersion in axial and radial direction for gas-phase, where pseudo-homogeneous reaction was considered instead of modelling internal transport. Schmidt et al. (2013) developed a steady state 2D model and regarded catalyst layer using a slab geometry. Internal diffusion was modeled while external diffusion was not considered. The literature review shows that wall-coated microchannel reactors are often considered to be operated under laminar flow conditions (Kolb and Hessel, 2004; Kiwi-Minsker and Renken, 2005; Walter et al., 2005).Walter et al. (2005) observed that the application of plug flow model to determine kinetics was validated with a dynamic 2D model, including axial and radial dispersion. In summary, due to thin catalyst layer and small diameter of the channel, plug flow conditions can usually be assumed in the microchannel reactors.

The aim of this research is to combine modelling of industrially relevant reaction of a bio-component to general modelling methodology development of microchannel reactors. New insights to the detailed mechanistic modelling of 1-butanol dehydration network on γ-Al_2O_3 will be introduced. Microchannel reactor advantages related to mass and heat transfer are utilized by determining intrinsic kinetics for 1-butanol dehydration reaction based on experiments in a coated microchannel reactor. Furthermore, simulations are performed by developing a dynamic 2D model considering mass transport inside the catalyst layer to determine optimal operation parameters, for instance, catalyst coating thickness and reactant partial pressure.

2. Experimental part

2.1. Kinetic experiments

Sandwich-type structured microchannel reactors composed of two plates coated with pure γ-alumina catalyst were used in the dehydration of 1-butanol to butenes and dibutyl ether. The plates (14 channels, width 500 μm and depth 250 μm, see Figure 4) were obtained from IMM (Institute fr Mikrotechnik Mainz Gmbh, Germany). The reactor contained 18 mg of catalyst, 9 mg per plate. The coating method has been described elsewhere (Zapf et al., 2003). The catalyst coated plates were calcined at 600 °C for two hours.

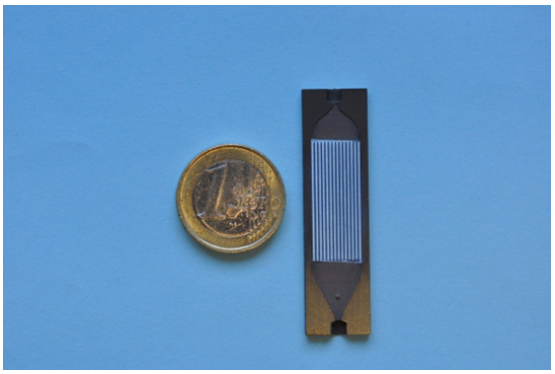

Figure 4 Microchannel reactor plate with dimensions, diameter 500μm, depth 250μm and length 25 mm.

1-Butanol (VWR, 99.9 %) was fed to reactor with HPLC-pump (Agilent Technologies 1100 Series Isocratic pump) via evaporator with inert argon (AGA, 99.999 %) flow. 1-Butanol/Ar ratio was varied in the experiments. Reaction products were analyzed by an online Fourier transform infrared spectrometer (FTIR, Gasmet Cr-2000, Temet Instruments). The flow was diluted with nitrogen (AGA, 99.999 %) before analysis to achieve the flow required by the analysis equipment.

The microreactor experiments were carried out in a temperature range 346 – 397 °C. The typical length of the experiment was 4 hr; some longer experiments (20 h) were performed to examine the stability of the catalyst. Between the experiments catalyst regeneration was performed with constant air flow of 30 ml/min at 550 °C for an hour. The experimental parameters are shown in Table 1.

2.2. Validation of kinetic operation regime and selection of reactor model

Many authors in literature have reported advantages of applying microchannel reactors (Kolb and Hessel,

Table 1 Experimental conditions

Variables	Ranges
$C_{C_4H_9OH}$	1.3−3.4 mol/m^3
	(partial pressure 7.5−20.4 kPa)
Temperature	346 – 397 °C
Flow rate (C_4H_9OH)	0.075−0.2 ml/min
Catalyst amount	18 mg
Weight hourly space velocity	195−521 h^{-1}

2004; Görke et al., 2009). Görke et al. (2009) reported that applying a wall coated microchannel reactor provides the opportunity to determine kinetics without mass and heat transfer considerations. Thus different empirical correlations can be employed to identify if both external and internal mass transport resistances can be neglected in the estimation of kinetic parameters.

For wall coated microchannel reactors Mears criterion for external mass transfer (Mears, 1971) is modified by Görke et al. (2009) and has been successfully validated by Lopes et al. (2011).

$$\frac{r_{eff,obs}\frac{V_{cat}}{O_{cat,geo}}}{k_g \cdot C_{i,bulk}} < \frac{0.05}{n} \tag{1}$$

Where $r_{eff,obs}$ is the observed reaction rate, V_{cat} is volume of the catalyst, $O_{cat,geo}$, is the catalyst geometric surface area, k_g is the mass transfer coefficient and $c_{i,bulk}$ is the inlet concentration of the reactant. The mass transfer coefficient k_g can be replaced by the ratio of diffusion coefficient D_i to diffusion pathway. The diffusion pathway is difference between the channel radius $r_{channel}$ and layer thickness δ_{cat}. If the criterion is fulfilled then mass transfer in the boundary layer is not present. (Pfeifer, 2012).

$$\frac{r_{eff,obs}(r_{channel} - \delta_{cat})\frac{V_{cat}}{O_{cat,geo}}}{D_i \cdot C_{i,bulk}} < \frac{0.05}{n} \tag{2}$$

Modified Weisz-Prater criterion for coated microchannel reactors is applied to estimate mass transfer (pore diffusion) inside the catalyst layer (Pfeifer, 2012).

$$\frac{r_{eff,obs}(\frac{V_C}{O_C})^2}{D_i^{eff} \cdot C_{i,bulk}} < 0.1, \eta > 0.95, n \neq 0 \tag{3}$$

Where, D_i^{eff} is the effective diffusion coefficient in catalyst layer, $C_{i,g}$ is the concentration of species at the surface of the catalyst and n is the reaction order.

The binary diffusion coefficient of $C_{C_4H_9OH}$ in Ar was calculated to be $1.34{\cdot}10^{-6}$ and effective diffusivity for $C_{C_4H_9OH}$ in the catalyst layer was calculated to be $1.8{\cdot}10^{-7}$. Using these empirical correlations in Equations 1 – 3, it is observed that both external and internal mass transport resistances are not present for the range of experimental conditions (Table 2). The L.H.S of Equation 2 was evaluated to be $4.5{\cdot}10^{-5}$ and L.H.S of Equation 3 was evaluated to be $2.5{\cdot}10^{-4}$.

Table 2 Set of values used for evaluation of mass transfer criteria

Gas flow l/min	δ_{cat} μm	Re	Sc
0.048	25	39.09	32.31
0.145	25	9.37	32.31

Thus parameter estimation can be carried out by applying a steady state 1D-pseudo-homogeneous plug flow model.

$$\frac{dc_i}{dx} = \tau\rho_b \sum v_{ij}R_j \tag{4}$$

2.3. Parameter estimation strategy

In order to reduce the number of parameters to be estimated, the chemical equilibrium of individual reactions in the selected reaction scheme was studied (presented in Section 3.2). ReaEqu module in Flowbat software (Jakobsson et al., 2014) was used to compute equilibrium for multiple reactions in a wide temperature range. In Flowbat software, thermodynamic properties are retrieved from the Design Institute for Physical Properties (DIPPR) database. For kinetics of the reactions, empirical power law and surface reaction mechanism based models were applied.

Parameter estimation was performed by using MATLAB® software. Minimization of Residual Sum of Squares (RSS) was achieved by Nelder-Mead simplex algorithm. For solving ordinary differential equations, ODE15s solver was used. Objective function Q_p was minimized using non-linear regression.

$$Q_p = min \sum_{i}^{nm} (y_{exp} - y_{cal})^2 \tag{5}$$

Mean temperature averaging methodology was used to obtain rate constant at the average temperature. By this technique experiments are centralized and the correlation between parameters is suppressed.

$$k = \overline{k} e^{\frac{E_a}{R}\frac{1}{\theta}} \tag{6}$$

Where $\overline{k}$ is the rate constant at average temperature $\overline{T}$ and θ is defined as,

$$\frac{1}{\theta} = \frac{1}{T} - \frac{1}{\overline{T}}. \tag{7}$$

3. Results

3.1. Results from MCR experiments

Different reaction products were detected in the product gas where 1-butene, water, dibutyl ether were observed as main products but also cis-2-butene, trans-2-butene and isobutene which are formed in small amounts from 1-butene by isomerisation according to Figure 5. At reaction temperatures above 390 °C and 1-butanol partial pressure $< 13kPa$, high selectivity ($>$ 90%) to 1-butene was achieved. Formation of dibutyl ether was very low up to 5% of the products. Butene isomers, cis-2-butene, trans-2-butene and isobutene were also observed in lower quantities, less than 4% of formed product. For reaction temperatures below 380 °C and butanol partial pressure > 13 kPa, formation of dibutyl ether was increased up to 10% and as high as 14% at temperatures of 346 °C. Furthermore, temperature did not affect the butene isomers distribution that significantly.

The thermodynamics to a certain extent dictates the selection of temperature to achieve high yields of butenes as a reaction product. High temperatures favor the direct dehydration route to 1-butene. If butenes are the desired products then in order to suppress ether formation the partial pressure has to be kept low. From experiments it was observed that at temperatures > 380 °C and the partial pressure of 1-butanol < 13 kPa, high selectivity to 1-butene ($>$ 90%) was achieved. This can be explained by the fact that at low partial pressure the molecules occupy far away catalyst sites and due to low concentration of 1-butanol in the bulk, possibility to form dibutyl ether is low (Phung et al., 2014). Similarly if dual site mechanism is considered to form dibutyl ether, it can be postulated that since the molecules are occupied on scattered catalyst sites the possibility of interaction between two adsorbed species at adjacent sites is very low (Berteau et al., 1985). Increasing the partial pressure in turn increases the concentration of butoxy species formed by adsorption of 1-butanol on the active sites. The concentration of 1-butanol in bulk gas is also high in a continuous flow reactor as compared to a batch reactor, where it would decreases with time. Whereas, when the reaction temperatures are comparatively lower, then due to thermodynamics the possibility to form dibutyl ether becomes higher as compared to butene (Berteau et al., 1985, 1991).

To determine kinetics of the reaction system, the observations from experiments and studies reported in literature for 1-butanol dehydration on alumina (Berteau et al., 1985) and ethanol dehydration on alumina (Phung et al., 2014), were considered. Two types of kinetic models, a more general power law kinetics and detailed surface surface reaction mechanism were considered for describing the reaction kinetics. Butene isomers have been discarded due to very low percentage in the product gas, and thus were lumped together with 1-butene. For determining kinetics through power law, based upon the experimental observations and literature (Berteau et al., 1985), reaction scheme presented in Figure 5 has been suggested for 1-butanol dehydration on γ-Al_2O_3. This scheme considers reactions between the bulk species and leaves aside the catalytic action. The surface reactions in the system are introduced in Section 3.4.

3.2. Thermodynamic equilibrium study for reactions

Chemical equilibrium of individual reactions I, II, and III (presented in Figure 5); was evaluated with ReaEqu module in Flowbat software (Jakobsson et al., 2014). The obtained equilibrium constants, equilibrium conversions and reaction enthalpies as functions of temperature for these three different reactions are shown in Table 3.

The main reaction for dehydration of 1-butanol to 1-butene (reaction I) has a very high equilibrium constant, suggesting that at the studied temperature range this reaction can be considered as irreversible reaction. The second reaction leading to formation of dibutyl ether has a relatively low equilibrium constant and this reaction has to be considered as a reversible reaction. The third reaction, i.e, dissociation of dibutyl ether to 1-butene and water has a very high value for the equilibrium constant in the given reaction conditions. Thus this reaction is also considered as an irreversible reaction. The equilibrium conversion for reaction I in the experimental temperature ranges is 99.2 – 99.4% and the selectivity to 1-butene is 99.9%. Thus at higher temperatures, higher conversion of 1-butanol and high selectivity to 1-butene can be achieved. Although the residence times in the experiments did not allow achieving equilibrium conversions relatively high conversions (88%) were observed.

The thermodynamic values for the reaction enthalpy reveal that reactions I and III are endothermic reactions, whereas reaction II is an exothermic reaction. This implies that at high temperatures, high selectivity to butenes could be achieved. Van′t Hoff equation was applied for the reaction II to calculate equilibrium constant as a function of temperature. The equilibrium constant value is then used in kinetics to express the reaction rate of backward reaction.

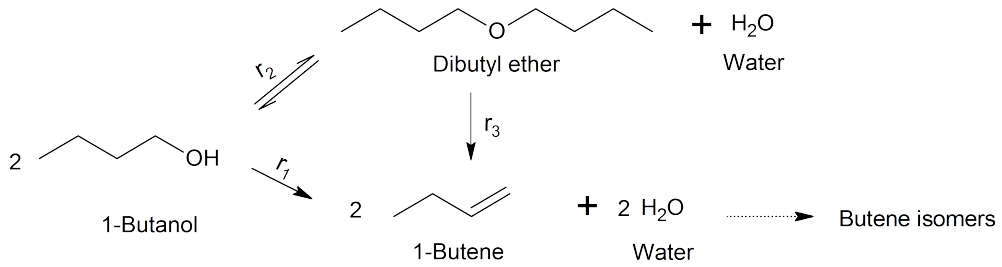

Figure 5 Proposed reaction scheme for 1-butanol dehydration over γ-alumina modified from (Berteau et al., 1985).

Table 3 Equilibrium constants of three reactions as function of temperature. Summing reactions II and III yields reaction I, and thus $K_1=K_2 \cdot K_3$, which is consistent with laws of thermodynamics.

Temperature (K)	K_{eq} for reactions			Equilibrium conversions			Equilibrium enthalpies (kJ/mol)		
	K_I	K_{II}	K_{III}	X_I	X_{II}	X_{III}	ΔH_I	ΔH_{II}	ΔH_{III}
613	14800	3.5	4269	0.992	0.651	0.985	34.26	-22.02	56.28
619	15800	3.3	4756	0.992	0.646	0.986	34.25	-21.96	56.22
625	16860	3.2	5287	0.992	0.641	0.986	34.24	-21.91	56.15
631	17960	3.1	5865	0.993	0.636	0.987	34.23	-21.85	56.08
637	19110	2.9	6492	0.993	0.632	0.988	34.22	-21.80	56.02
643	20300	2.8	7171	0.993	0.627	0.988	34.21	-21.74	56.95
649	21550	2.7	7906	0.993	0.623	0.989	34.20	-21.69	56.88
655	22850	2.6	8700	0.993	0.618	0.989	34.18	-21.63	56.82
661	24200	2.5	9555	0.994	0.614	0.990	34.17	-21.58	56.75
667	25610	2.4	10480	0.994	0.610	0.990	34.15	-21.53	56.68

3.3. Power law kinetics

The power-law approach with first order reactions is a classic first attempt to describe kinetic data. It allowed the comparisons with few existing literature results and was therefore tested and found successful in describing the observations. This implies that more intricate catalytic behavior could be reduced to a first order behavior in the studied regime. Berteau et al. (1985), have demonstrated the existence of different regimes for apparent reaction orders between zero and one. In the power law model the order is fixed to a constant one, whereas the mechanistic model in principle allows the reaction orders to vary depending on the conditions.

Using the reaction scheme in Figure 5 the rate equations were derived for the reactions in the system for applying power law kinetics. Reaction I and III were assumed to be irreversible and reaction II reversible based on studies of chemical equilibrium (Section 3.2). The rate equations for different reactions are thus presented below,

$$r_1 = k_1 \cdot c_A \tag{8}$$

$$r_2 = k_1 \cdot (c_A^2 - \frac{1}{K_{eq}} \cdot c_C \cdot c_D) \tag{9}$$

$$r_3 = k_3 \cdot c_D \tag{10}$$

where, A is 1-butanol, B is 1-butene, C is water and D is dibutyl ether.

The mass balances for species taking account the stoichiometry are given as,

$$\frac{dc_A}{d\tau} = (-2r_1 - 2r_2) \cdot \rho_b \tag{11}$$

$$\frac{dc_B}{d\tau} = (2r_1 + 2r_3) \cdot \rho_b \tag{12}$$

$$\frac{dc_C}{d\tau} = (2r_1 + r_2 + r_3) \cdot \rho_b \tag{13}$$

$$\frac{dc_D}{d\tau} = (r_2 - r_3) \cdot \rho_b \tag{14}$$

3.4. Kinetics based on surface reaction mechanism

As discussed previously in Section 1, the surface reaction mechanism is based on recent spectroscopic studies. In this mechanism surface butoxy species are considered as intermediates to butene and dibutyl ether formation. These reactive adsorption steps are considered to be in quasi-equilibrium. The identities of sites are presented in Figure 6.

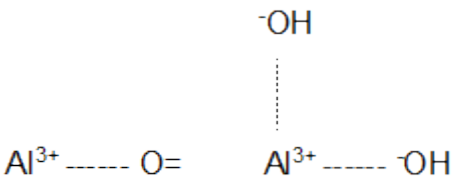

(a) Site 1: Lewis acid site (unsaturated cationic site).

(b) Site 2: surface hydroxyl bound to unsaturated cationic site.

Figure 6 Two different types of active sites considered on the surface of γ-Al_2O_3.

The ether formation is considered as reversible reaction where adsorbed ether on site 1 or site 2 may dissociate back into a butoxy and loosely hydrogen bonded alcohol. The butoxy species and alcohol may undergo the same reaction or it is also possible to form butene and gas−phase alcohol. The surface species and active sites are denoted by * sign to differentiate from bulk or gas phase species. The reaction equations are presented as,

$$Butanol + site1^* \leftrightarrow Butoxy^* \tag{15}$$

$$Butanol + site2^* \leftrightarrow Butoxy^* + water \tag{16}$$

$$H_2O + site1^* \leftrightarrow site2^* \tag{17}$$

Butene is formed from the surface butoxy species and site 2 is regenerated.

$$Butoxy^* \leftrightarrow Butene + site2^* \tag{18}$$

Ether formation through single site mechanism occurs with nucleophilic attack of the butoxy species on H−bonded undissociated butanol, with the site 2 regeneration.

$$Butoxy^* + Butanol \leftrightarrow DBE + site2^* \tag{19}$$

Considering dual site mechanism the overall equation for dibutyl ether can be written as,

$$2Butoxy^* \leftrightarrow DBE + site1^* + site2^*. \tag{20}$$

Overall site balance and site coverage can be give as,

$$N_{Butoxy} + N_1 + N_2 = N_{tot} \tag{21}$$

$$\theta_{Butoxy} + \theta_1 + \theta_2 = 1. \tag{22}$$

Surface coverage of butoxy species can be achieved by combining Equations 15 – 16 and 22 and assuming the steps in Equations 15 – 16 to be in quasi-equilibrium,

$$\theta_{Butoxy} = \frac{K_1 c_A}{1 + K_1 c_A + \frac{K_1}{K_2} c_C}. \tag{23}$$

The detailed derivation to achieve θ_{Butoxy} is provided in the Supplementary Information. The formation of butene from butoxy species is assumed to be rate determining step and the reaction rate equation for butene formation through Equation 18 is then written as,

$$r_1 = k_1.\theta_{Butoxy}. \tag{24}$$

The final rate equation is obtained when Equation 23 is inserted into Equation 24,

$$r_1 = k_1.\frac{K_1 c_A}{1 + K_1 c_A + \frac{K_1}{K_2} c_C}. \tag{25}$$

The derivation of the surface reaction mechanism for the formation of dibutyl ether also, expressing the backward rate constant by utilizing macroscopic thermodynamic equilibrium constants is less straightforward than for the power law kinetics. But it can be done as follows:

In single−site mechanism (from here on referred to as mechanistic model I) the nucleophilic attack of butoxy species on H-bonded undissociated butanol is assumed to be the rate determining step,

$$r_2 = k_2.(\theta_{Butoxy}.c_A - \frac{\theta^2_{Butoxy} c_C c_D}{K_{eq} c_A}). \tag{26}$$

The final rate equation for dibutyl ether with single−site mechanism is obtained when Equation 23 is inserted into Equation 29,

$$r_2 = k_2.\left(\frac{K_1 c_A}{1 + K_1 c_A + \frac{K_1}{K_2} c_C}.c_A - \frac{(\frac{K_1 c_A}{1+K_1 c_A+\frac{K_1}{K_2} c_C})^2 c_C c_D}{K_{eq} c_A}\right). \tag{27}$$

Considering dual site mechanism (from here on referred to as mechanistic model II) the rate equation for dibutyl ether can be written as,

$$r_2 = k_2.(\theta^2_{Butoxy} - \frac{\theta^2_{Butoxy} c_C c_D}{K_{eq} c_A^2}). \tag{28}$$

The final rate equation for dibutyl ether with dual site mechanism is obtained when Equation 23 is inserted into Equation 31,

$$r_2 = k_2.\left((\frac{K_1 c_A}{1 + K_1 c_A + \frac{K_1}{K_2} c_C})^2 - \frac{(\frac{K_1 c_A}{1+K_1 c_A+\frac{K_1}{K_2} c_C})^2 c_C c_D}{K_{eq} c_A^2}\right). \tag{29}$$

This version of proposed surface reaction mechanism contains two Arrhenius dependent rate constants and two adsorption equilibrium constants. The thermodynamic equilibrium constant is obtained from the thermodynamics study presented in Section 3.2. Consequently there are no more degrees of freedom in the surface reaction model compared to the power-law model. The difference is that mechanistic approach allows a change in the reaction order of butanol for 1-butene and ether formation depending on the reaction conditions: temperature and partial pressure of 1-butanol. This particular mechanistic feature has been advocated in literature (Berteau et al., 1985) even though it has not been used for determining kinetics of alcohol dehydration.

The mass balances for species taking account the stoichiometry are given as,

$$\frac{dc_A}{d\tau} = (-r_1 - 2r_2) \cdot \rho_b \tag{30}$$

$$\frac{dc_B}{d\tau} = (r_1) \cdot \rho_b \tag{31}$$

$$\frac{dc_C}{d\tau} = (r_1 + r_2) \cdot \rho_b \tag{32}$$

$$\frac{dc_D}{d\tau} = (r_2) \cdot \rho_b \tag{33}$$

where, again A is 1-butanol, B is 1-butene, C is water and D is dibutyl ether.

3.5. Parameter estimation results

Kinetic parameters estimated with pseudo-homogeneous plug flow model are presented in Table 4. The estimated parameters are physically meaningful and relatively close to the ranges reported for activation energies in literature Table 4. Both power law kinetics and surface reaction mechanism based kinetics were able to describe the kinetics of the dehydration reaction. Coefficient of determination R^2 for estimated parameters from power law and mechanistic models I and II is about 99%, which is in good correspondence.

The parameter values are compared to the two literature references. Makarova (1994) used H-ZSM-5 with high concentration of acid sites in temperature range of 378−458 K, whereas, Clayborne et al. (2004) applied pure γ-alumina in Temperature Programmed Desorption (TPD) studies in temperature range of 500−620 K.

3.6. Model fit and sensitivity analysis

The obtained parameters are used to fit the model against experimental data with power law kinetics and mechanistic model I. Two plots are presented in Figure 7 using power law kinetics. Figure 7 (a) contains 1-butanol conversion as a function of temperature at WHSV of 521 h^{-1}, corresponding to residence time of 0.01s in the reactor. The partial pressure of 1-butanol was 14.6 kPa. Figure 7 (b) contains 1-butanol conversion as a function of different residence times at partial pressure of 12.2 kPa. The corresponding WHSV are indicated on the plots with '•' symbol for different residence times. The presented plots in Figure 7 show that the model reproduces the experimental data and shows a good fit.

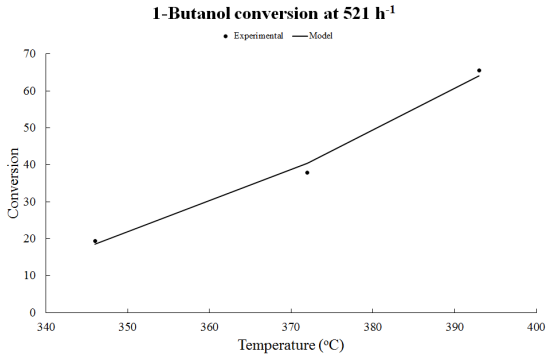

(a) Temperature vs. conversion of experimental and model values for WHSV 521 h^{-1} and 1-butanol partial pressure of 14.6 kPa.

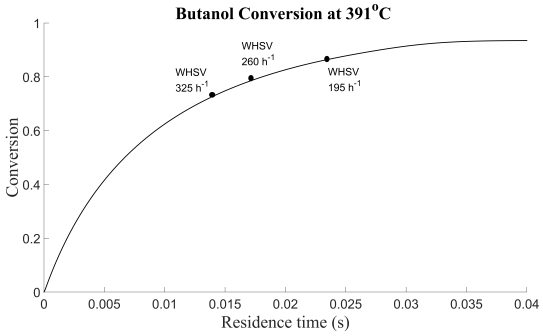

(b) Residence time vs. conversion plotted for 1-butanol partial pressure of 12.2 kPa and different WHSV. Experimental points for corresponding WHSV are denoted by •.

Figure 7 Model fit plot for 1-butanol conversion against temperature and WHSV (corresponding to residence time).

As observed in experiments, for reactions at higher temperatures resulting in high conversion of 1-butanol (> 60%), selectivity to 1-butene is also very high (90 – 98%). This indicates dominance of direct dehydration route via reaction I. Thus in order to perform the sensitivity analysis, the objective function is investigated in terms of parameters for reaction I only. Both rate

Table 4 Parameter estimation results with power−law and mechanistic models I and II. K_1 and K_2 are fixed adsorption parameters for the formation of butoxy species on site 1 and site 2.

Parameters	Model results			Literature	
	Power law	Mechanistic I	Mechanistic II	(Makarova, 1994)	(Clayborne et al., 2004)
E_1 (kJ/mol)	135	134.6	135.7	134	132
A_1 (1/s)	$5.44{\cdot}10^{9}$	$1.73{\cdot}10^{10}$	$2.66{\cdot}10^{10}$	$1.92{\cdot}10^{15}$	$1.1{\cdot}10^{8}$
E_2 (kJ/mol)	102	105	100	92	100
A_2 (1/s)	$6.87{\cdot}10^{5}$	$3.91{\cdot}10^{6}$	$8.68{\cdot}10^{8}$	$3.1{\cdot}10^{10}$	$1{\cdot}10^{6}$
E_3 (kJ/mol)	130	$K_1 = 1.3$	$K_1 = 0.6$	134	-
A_3 (1/s)	$2.93{\cdot}10^{9}$	$K_2 = 0.55$	$K_2 = 0.525$	$4.5{\cdot}10^{10}$	-

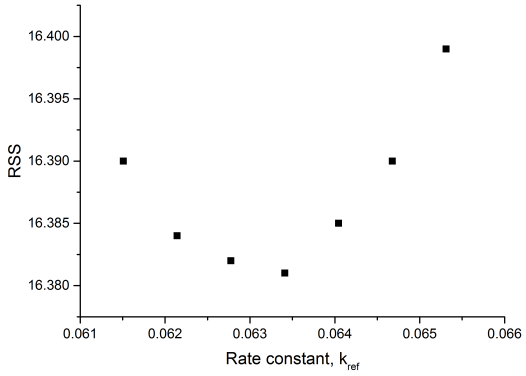

(a) Normalized reaction rate constant plotted against objective function.

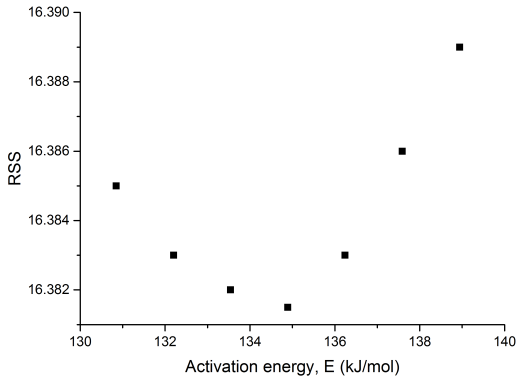

(b) Activation energy plotted against objective function.

Figure 8 Parameter sensitivity analysis for reaction I with power-law kinetics.

constant (k) and activation energy (E) are varied individually, while all other estimated parameters are kept constant. Graphical representation is shown in Figure 8, where symmetry was observed on both sides and minimum value for the objective function was achieved in the vicinity of estimated values of the parameters. Similar fits were also observed for surface reaction mechanism models. The R^2 value was observed around 99% and sensitivity analysis also produced model fits in confidence intervals as observed for power law kinetics. These figures are presented in Supplementary Information: Additional Figures.

3.7. Dynamic 2D model

3.7.1. Microchannel reactor

A dynamic 2D heterogeneous model was developed for Microchannel Reactor (MCR) to study mass transport limited and kinetically controlled regimes.

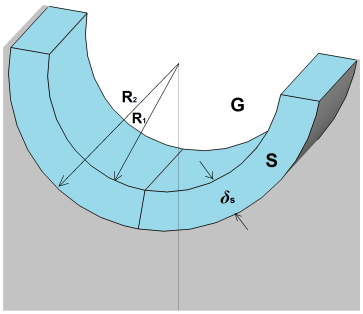

Figure 9 Cross section of the half cylindrical channel. R_1 is the radii of inner cylinder, R_2 is the radii of outer cylinder, δ_s is the difference between the two radii and corresponds to the deoposited catalyst (S) layer thickness. G represents gas-phase in the free channel.

The microchannel reactor is assumed to have uniform conditions in parallel channels and thus a single channel can be modeled to represent all the channels in reactor domain. Inside the channel empty space, plug flow is used to the mass transport implying radially good mixing. Diffusion and reaction in the porous coating on the channel walls take place via heterogeneously catalyzed gas-phase reactions. For modelling purposes, the channel is assumed to consist of two hollow cylinders inside

each other with internal radii R_1 and R_2, where the internal cylinder corresponds to the empty channel space and the difference between the radii of the two cylinders contains the catalyst layer (Figure 9).

The following assumptions are made for the single channel model:

- Isothermal conditions: Isothermal conditions are assumed throughout the channel and the catalyst layer.
- Constant pressure: There is no pressure drop across the length of the reactor.
- No homogeneous reaction: In the gas phase no reaction takes place. Reactions are heterogeneously catalyzed in solid catalyst layer.
- Ideal gas: The gas mixture has an ideal gas behavior at reaction conditions.
- External mass transfer: External mass transfer resistances are neglected based on Mears criterion (Görke et al., 2009), presented in Section 2.2, and the surface concentration was set to correspond to the bulk concentration.

The detailed derivations for the mass balances in the channel domain and in the catalyst layer are provided in the Supplementary Information. However, the main mass balance equations, boundary conditions and transport properties are also discussed in this section.

Mass balance in the cylindrical coating for each component can be described as follows:

$$\epsilon_p \frac{\partial c_i}{\partial t} = \frac{D_{ei}}{R_1^2}\left(\frac{\partial^2 c_i}{\partial z^2} + \frac{1}{z}\frac{\partial c_i}{\partial z}\right) + r'\rho_p. \tag{34}$$

where $z = r/R_1$, is a dimensionless radial coordinate

The boundary conditions applied to the surface and bottom of the layer are,

$$c_i(r = R_1) = c_{i,gas}(x), \qquad \frac{\partial c_i(r = R_2)}{\partial r} = 0, \tag{35}$$

and following initial conditions at t=0 were assumed

$$c_i^s = c_i^{Go}. \tag{36}$$

Dynamic mass balance in the free gas channel for each component obtains the following form:

$$\frac{\partial c_i}{\partial t} = -\frac{U}{L\epsilon_b}\frac{\partial c_i}{\partial x} - \frac{2D_e}{R_1^2\epsilon_b}\frac{\partial c_i}{\partial z}\bigg|_{z=1}. \tag{37}$$

Where $x = l/L$, is a dimensionless axial coordinate

The boundary condition applied to the free channel domain is,

$$c_i(l = 0) = c_{i,gas}(in) \tag{38}$$

and the initial condition for mass balances in free channel at t=0 can be written as:

$$c_i^G = c_i^{Go} \tag{39}$$

The effective diffusion coefficient D_{ei} of components were estimated by using Wilke approximation

$$D_{ei} = (\frac{\epsilon}{\tau})D_i \tag{40}$$

$$D_i = \frac{1 - x_i}{\sum_{k=1}^{N} \frac{x_k}{D_{ik}}} \tag{41}$$

Binary molecular diffusion coefficients D_{ik} used in Wilke equation were estimated using Fuller-Schettler-Giddings (Fuller et al., 1966) equation.

$$D_{ik} = \frac{T^{1.75} \cdot \sqrt{\frac{1}{M_i} + \frac{1}{M_k}}}{P \cdot (v_i^{1/3} + v_k^{1/3})} \cdot 10^{-7} m^2/s \tag{42}$$

The volume contributions of the molecules were obtained from literature (Poling et al., 2000).

3.7.2. Packed bed powder reactor

Analogous continuum models were expressed for PBR as well (for details see Supplementary Information).

Mass balance in catalyst particle for each component is given as follows,

$$\epsilon_p \frac{\partial c_i}{\partial t} = \frac{D_{ei}}{R_p^2}\left(\frac{\partial^2 c_i}{\partial z^2} + \frac{2}{z}\frac{\partial c_i}{\partial z}\right) + r'\rho_p \tag{43}$$

where $z = r/R_p$, is the dimensionless radial coordinate.

Following boundary conditions,

$$\frac{\partial c_i(r = 0)}{\partial r} = 0, \qquad c_i(r = R_p) = c_{i,gas}(x) \tag{44}$$

and initial conditions at t=0 were used.

$$c_i^s = c_i^{Go} \tag{45}$$

Mass balance in the reactor for each component can be expressed

$$\frac{\partial c_i}{\partial t} = -\frac{U}{L\epsilon_b}\frac{\partial c_i}{\partial x} - \frac{3D_e(1 - \epsilon_b)}{R_p^2\epsilon_b}\frac{\partial c_i}{\partial z}\bigg|_{z=1} \tag{46}$$

where $x = l/L$ is dimensionless, axial coordinate, following boundary condition,

$$c_i(l = 0) = c_{i,gas}(in) \tag{47}$$

and initial conditions at t=0, were used.

$$c_i^G = c_i^{Go} \tag{48}$$

The effective diffusivity of components is estimated by using Equations 40 – 42 presented in Section 3.7.1. In packed-bed reactor, catalyst particles of standard size between 250 – 420 μm were assumed. The concentration profile for 1-butanol was simulated with the developed 2D heterogeneous model.

3.7.3. Numerical solution strategy

Continuum equations leading to coupled partial differential equations were solved numerically in MATLAB® environment by method of lines, i.e., discretizing the system by approximating the axial and radial derivatives by backward and central differences, respectively. Discretization was done equidistantly and system matrices were developed accordingly. Achieved sparse matrix from the ODE system was manipulated to a diagonal matrix to make calculations computationally more efficient.

3.7.4. 2D MCR simulations

The concentration profiles inside the catalyst layer were simulated with the developed 2D dynamic model and the determined parameters. The thickness of the catalyst layer varies across the cylindrical cross-section; such that the layer is thin at the channel side-walls, whereas, the layer is thicker at the bottom of the channel. The Scanning Electron Microscopy (SEM) studies showed that the catalyst layer distribution varies between 15 μm to 30 μm, therefore the whole range was considered for simulations.

Concentration profile for 1-butanol inside the catalyst layer for different thicknesses is presented in Figure 10. The model simulations show that the reactant concentration profile starts to change significantly from layer thickness of 40 μm. With increase in the layer thickness beyond 40 μm, the concentration of the reactant inside the layer starts to decrease appreciably. This decrease in the concentration of the reactant along the dimensionless distance inside the catalyst layer with increased layer thickness, would result in decreased efficiency for the MCR. Thus more catalyst loading might not be a solution to achieve higher conversions. In order to fully utilize advantages of MCR rather a balance should be achieved between catalyst layer thickness, catalyst loading and conversion.

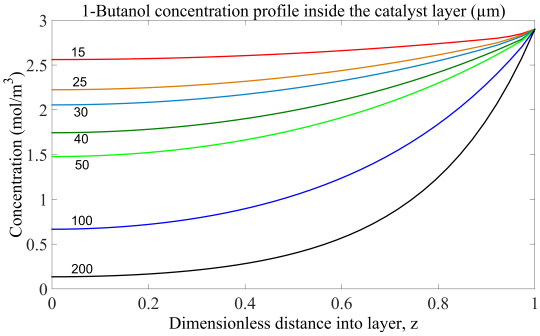

Figure 10 Simulated 1-butanol concentration profile inside the catalyst layer for different layer thicknesses at 391 °C. The higher catalyst layer thicknesses 100 and 200 μm correspond to ranges of radius for the standard particle size used in packed-bed reactor simulations.

To further validate the effect of concentration distribution inside the catalyst layer with varied layer thickness, the effectiveness factor was calculated for the first reaction. The effectiveness factor for cylindrical catalyst layer is considered analogous to the cylindrical shaped catalyst particle geometry. Considering characteristic length for the channel geometry, the effectiveness factor for any geometry can be written as,

$$\eta_{ei} = \frac{\tan(\phi_i)}{\phi_i}, \tag{49}$$

where Thiele modulus is calculated from equation

$$\phi_i = R_p \sqrt{\frac{k c_i^{n-1}}{D_{ei}}}. \tag{50}$$

Table 5 Effectiveness factor for the dehydration reaction to butene.

Catalyst layer thickness μm	Effectiveness factor η
15	0.97
25	0.93
30	0.91
40	0.85
50	0.79
100	0.52
200	0.27

The effectiveness factor η (Table 5) varies between 0.97-0.91 as a function of catalyst layer thickness variation (15−30 μm). This shows that for an average layer

thickness of 25 μm, diffusional limitations are minor and microchannels can be considered to operate in the kinetic regime. The effectiveness factor is decreased significantly with increasing thickness of the catalyst layer and reaction is considerably affected by the pore diffusion for layer thicknesses of 100 μm and beyond which equals the particle size of the catalyst in the packed-bed reactor. Thus the findings of the 2D simulations presented in Figure 10 agree with the effectiveness factor.

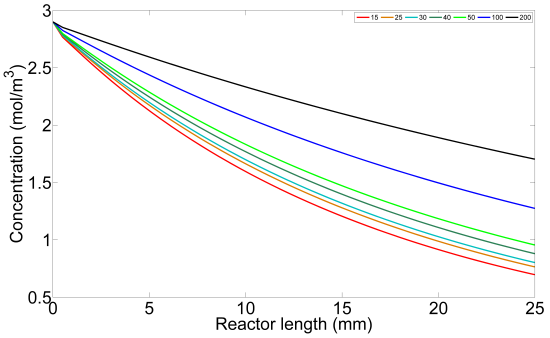

Figure 11 Simulated 1-butanol concentration profile across the reactor length for different layer thicknesses at 391 °C.

Bulk concentration profile along the axial coordinate is investigated with constant mass of catalyst for different layer thicknesses. The profile in Figure 11, shows that as the layer thickness is increased from 15 μm, the conversion is decreased and more reactant is available in the bulk phase. At lower catalyst layer thickness of 15 μm, the reactant is able to penetrate through to the layer and accesses the whole catalyst layer. Thus more reactant is transported from surface to the catalyst layer and reactant distribution inside the layer is sufficient enough to lead to high conversion which in turn means that the concentration of the reactant in the bulk would be lower. On the other hand increased catalyst layer thickness means increased resistance to the transport of the reactant within the catalyst layer, therefore within a set residence time the reactant conversion is low and respectively the bulk concentration is higher.

3.8. Comparison of MCR and PBR

Concentration profiles of 1-butanol inside the catalyst layer for average thickness of 25 μm and in PBR using spherical particles of radius ranging from 100 – 210 μm are shown in Figure 12. The catalyst mass in both the reactors is considered to be 18 mg.

As observed in Figure 12, 1-butanol concentration inside the spherical catalyst particle considering particle size with diameter 200 – 420 μm show that internal resistance to mass transport are present in PBR. In comparison, for MCR with average layer thickness of 25 μm internal mass transport resistances are very low and the catalyst in the entire layer is accessible to the reactant. Thus within experimental conditions, internal mass transport resistance can be avoided in MCR as compared to PBR, where particle size cannot be progressively reduced owing to emerging pressure drop along the catalyst bed.

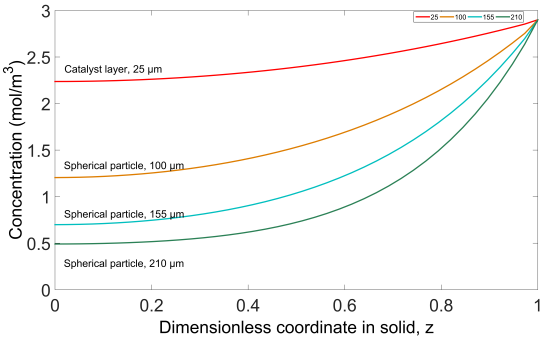

Figure 12 Simulated 1-butanol concentration profile inside MCR with layer thickness 25 μm and PBR with spherical particle radius of 100 μm, 155 μm and 210 μm at 391 °C.

The role of the catalyst layer thickness is very important and has a twofold impact on the reaction process. The MCR simulations revealed that if the catalyst layer deposited on the inner walls of the microchannel reactor is thicker than 40 μm the advantages related to mass transfer and heat transfer may not be fully realized with the application of MCR. The presence of mass transfer resistance due to high catalyst layer thickness would affect the distribution of the reactant concentration across the catalyst sites and the catalyst pores would be less accessible to the reactant further away from surface and closer to the channel walls. This in turn would decrease the overall conversion of the process. On the other hand thinner catalyst layer would result in decreased catalyst loading in the channels which is often attributed a problem in microchannel reactors as compared to packed-bed reactors.

Another important aspect to understand is whether the increased diffusion limitations induced by increased layer thickness in the reactor would impact the selectivity to 1-butene or dibutyl ether by utilizing the other optimized reaction parameters (partial pressure, residence time, and temperature). At optimized conditions for high selectivity to 1-butene, such as, low partial pressure of 1-butanol, high residence time and high reac-

tion temperatures, it may be postulated that due to thermodynamics and reaction pathway (intermediate butoxy species, single-site mechanism), the selectivity to 1-butene may not be affected significantly, which was also observed in simulations. It is pertinent to mention that selectivities of 1- butene and dibutyl ether are coupled to each other and thus increasing or decreasing the selectivity to either one would be vice versa on the other product.

The selectivity to dibutyl ether at the catalyst layer surface, may still not be affected due to abundance of adsorbed and gas phase 1-butanol close to the surface, at optimized conditions, i.e., high partial pressure of 1-butanol, low residence time and low reaction temperatures. The surface reaction mechanisms for ether formation (single-site and dual-site) are favored due to abundance of adsorbed butoxy species at the surface and 1-butanol in gas phase close to the surface. However, deeper within the catalyst layer due to lack of gas phase 1-butanol as well as adsorbed butoxy species, possibility to form ether through single site interaction with 1-butanol within the pore (single-site mechanism) and the interaction of two neighboring butoxy species (dual-site mechanism), would be limited. This may result in decreased selectivity to dibutyl ether, whereas 1-butene selectivity would increase. This deviation in the selectivities was observed to be between 1−3 % from simulation results.

To achieve equilibrium conversions with the proposed 2D model, the reaction system was simulated with optimized parameters to assess and predict reactor performance at conditions beyond those of the experiments. The temperature was selected to be 391 °C (maximum temperature in experiments), partial pressure was kept >13 kPa to remain in region where reaction order change would not affect the power-law model. Furthermore, at the selected WHSV of 195 h^{-1} the residence time was doubled to see if the reaction system would achieve equilibrium conversion. The results for simulations with both power law and surface reaction scheme I are presented in Figure 13. Both models predict high conversions in the vicinity of the experimentally observed conversions for 1-butanol. The selectivity to 1-butene is high (> 90%) and dibutyl ther formation is observed up to 7% for the mechanistic model and 3% for the power-law model. This clearly shows that mechanistic model over-predicts the formation of dibutyl ether. This could be due to the fact that the mechanistic models lack an additional reaction route for conversion of formed dibutyl ether as compared to the power-law model. The temperature dependencies of the two adsorption constants K_1 and K_2 were omitted for simplicity and constant values were assigned compromising over the whole temperature range. Thus the mechanistic models would require its parameters to be determinded with more richer range of data and inclusion of temperature effect on the adsorption constants.

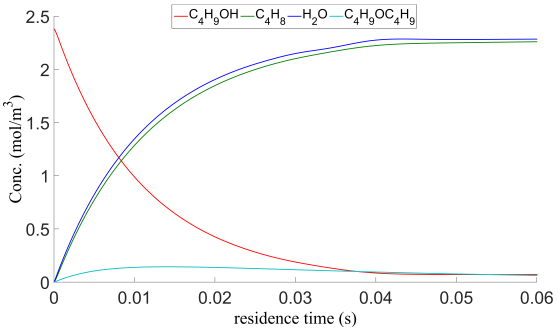

(a) Simulation results with power-law kinetics.

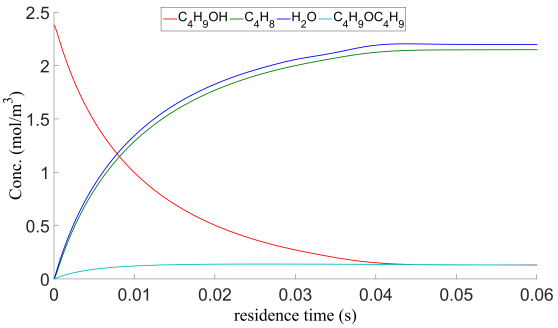

(b) Simulation results with mechanistic model I.

Figure 13 Concentration profiles of 1-butanol, butene, water and dibutyl ether, simulated with proposed model Equations 34 – 42, using reaction mechanism model and power-law kinetics, at reaction temperature 391 °C , partial pressure 15 kPa and longer contact time > 0.06 s.

Doubling the residence time did not yield equilibrium conversion for the simulated set of parameters. To further verify the equilibrium conversion the temperature was increased to 400 °C while keeping the partial pressure at 15 kPa and simulating for a longer residence time up to 0.06 s. The simulation results (presented in Supplementary Information: Additional Figures) show that the reaction system does reach the equilibrium conversion at 400 °C with power-law kinetics and 410 °C with surface reaction kinetics, keeping the residence time of 0.06 s as compared to 0.03 s in the experiments.

4. Conclusions

Kinetics of 1-butanol dehydration was addressed in alumina-coated microchannel reactor. Well-established

criteria (Mears and Weisz-Prater) were evaluated to confirm that the experiments were carried out in a kinetically controlled regime. Different ranges of conversions (18 – 88%) were achieved for varying experimental conditions. At temperatures > 391 °C high conversions (> 60%) of 1-butanol at different Weight Hourly Space Velocity (WHSV) were achieved in the coated microchannel reactor used in this study. Direct dehydration route to 1-butene was dominating and thus high selectivity to 1-butene was obtained in Microchannel Reactor (MCR).

A power-law type of kinetic model as well as a mechanistic model inspired by the current view of alumina-catalyzed alcohol dehydration mechanisms were tested against experimental data. Equal compatibilities to the data were found for the models in the studied conditions. Kinetic parameters were in a physically meaningful order of magnitude and agreed with earlier findings.

The determined kinetics were applied to simulate a microchannel reactor and a packed bed powder reactor. The proposed 2D simulation model for MCR validates that for catalyst layer thickness up to 40 μm, diffusional resistances are minimal and the effectiveness factor remains high up to 0.90. Increasing the layer thickness beyond 40 μm induces more considerable internal transport resistance. Simulations also validate that high selectivity to 1-butene is achieved with optimizing the reaction parameters, for instance, temperature and partial pressure of 1-butanol. Further simulations with the optimized reaction parameters for MCR revealed that packed-bed reactor with spherical catalyst particles of 250 – 420 μm diameter exhibits more significant internal mass transport resistance and lower effectiveness than MCR. The results demonstrate that MCR is a convenient tool for assessing reaction kinetics and potential for efficient production of chemicals. Valid MCR simulation model including adequate kinetic description allows optimization of the yield of desired product by choosing the operation parameters.

Acknowledgements

Academy of Finland is gratefully acknowledged for funding via research grant and Academy research fellowship of J.K. Mr. K. Kanervo is thanked for checking and revising the mathematical derivations.

Nomenclature

c	concentration ($mol \cdot m^{-3}$)
$c_{(i,bulk)}$	concentration in the gas bulk phase ($mol \cdot m^{-3}$)
$c_{(i,g)}$	concentration in to the gas phase at catalyst surface ($mol \cdot m^{-3}$)
$c_{(i)}^{Go}$	concentration of gas species in bulk at time t=0 ($mol \cdot m^{-3}$)
$c_{(i,g)}^{s}$	concentration of gas species at catalyst surface ($mol \cdot m^{-3}$)
D_i	molecular diffusivity ($m \cdot s^{-2}$)
D_{ei}	effective diffusion coefficient ($m \cdot s^{-2}$)
D_{ik}	binary diffusion coefficient ($m \cdot s^{-2}$)
δ_{cat}	catalyst layer thickness (μm)
E	activation energy (kJ/mol)
ϵ	catalyst layer porosity
ϵ_b	void fraction in channel
ϵ_p	catalyst particle porosity
η	effectiveness factor
k	reaction rate constant ($m^3 \cdot mol^{-1} \cdot s^{-1}$)
k_g	mass transfer coefficient ($m \cdot s^{-1}$)
$\overline{k}$	reaction rate constant at reference temperature ($m^3 \cdot mol^{-1} \cdot s^{-1}$)
M_i	molecular mass ($g \cdot mol^{-1}$)
n	reaction order
N	Notation for site balance
$O_{(Cat,geo)}$	catalyst geometric surface area (m^2)
P	pressure (bar)
ϕ	notation for surface coverage of species
Q_p	objective function
$r_{channel}$	radius of the microchannel (m)
R	general gas constant ($J \cdot mol^{-1} \cdot K^{-1}$)
R_1	radius of inner cylinder (m)
R_2	radius of outer cylinder (m)
r'	rate of reaction ($mol \cdot kg^{-1} \cdot s^{-1}$)
ρ_B	bulk density ($kg \cdot m^{-3}$)
ρ_p	catalyst particle density ($kg \cdot m^{-3}$)
$r_{(eff,obs)}$	observed volumetric reaction rate ($mol \cdot m^{-3} \cdot s^{-1}$)
R_e	Reynold number
S_c	Schmidt number
T	reaction temperature
$\overline{T}$	average reaction temperature (K)
τ	catalyst layer tortuosity
τ	space time
θ	thiele modulus
V_{Cat}	catalyst volume (m^3)
v_i	volume contributions of molecules
y_{exp}	experimental data point
y_{cal}	model value
A	subscript for 1-butanol
B	subscript for 1-butene
C	subscript for water
D	subscript for dibutyl ether

References

Bautista, F., 1995. 1-Butanol dehydration on $AlPO_4$ and modified $AlPO_4$: catalytic behaviour and deactivation. Appl. Catal. A Gen. 130, 47–65.

Bernal, S., Trillo, J., 1980. Selectivities of rare earth oxide catalysts for dehydration of butanols. J. Catal. 66 (1), 184–190.

Berteau, P., Delmon, B., 1989. Modified Aluminas : Relationship between activity in 1-butanol dehydration and acidity measured by NH_3 TPD. Catal. Today 5, 121–137.

Berteau, P., Delmon, B., Dallons, J.-L., Van Gysel, A., 1991. Acid-base properties of silica-aluminas: use of 1-butanol dehydration as a test reaction. Appl. Catal. 70 (1), 307–323.

Berteau, P., Ruwet, M., Delmon, B., 1985. Reaction Pathways in 1-Butanol Dehydration on γ-Alumina. Bull. des Sociétés Chim. Belges 94 (11-12), 859–868.

Busca, G., 2014. The surface of transitional aluminas: A critical review. Catal. Today 226, 2–13.

Chakor-Alami, A., Hindermann, J. P., Kiennemann, A., 1984. Dehydration of alcohols on iron Fischer-Tropsch type catalysts. React. Kinet. Catal. Lett. 26, 391–398.

Chen, C., Wang, L., Xiao, G., Liu, Y., Xiao, Z., Deng, Q., Yao, P., 2014. Continuous acetone-butanol-ethanol (ABE) fermentation and gas production under slight pressure in a membrane bioreactor. Bioresour. Technol. 163, 6–11.

Chen, G., Li, S., Jiao, F., Yuan, Q., 2007. Catalytic dehydration of bioethanol to ethylene over TiO_2/γ-Al_2O_3 catalysts in microchannel reactors. Catal. Today 125, 111–119.

Clayborne, P. A., Nelson, T. C., DeVore, T. C., 2004. Temperature programmed desorption-FTIR investigation of C_1-C_5 primary alcohols adsorbed on γ-Al_2O_3-alumina. Appl. Catal. A Gen. 257, 225–233.

Decanio, E. C., Nero, V. P., Bruno, J. W., 1992. Identification of alcohol adsorption sites on γ-alumina. J. Catal. 135, 444–457.

Delsarte, S., Grange, P., 2004. Butan-1-ol and butan-2-ol dehydration on nitrided aluminophosphates: Influence of nitridation on reaction pathways. Appl. Catal. A Gen. 259, 269–279.

Fuller, E. N., Schettler, P. D., Giddings, J. C., May 1966. New method for prediction of binary gas-phase diffusion coefficients. Ind. Eng. Chem. 58 (5), 18–27.

Giniestra, A. L., Patrono, P., Berendelli, M., Galli, P., Ferragina, C., Massucci, M., 1987. Catalytic activity of zirconium phosphate and some derived phases in the dehydration of alcohols and isomerization of butanes. J. Catal. 103, 2857–2862.

Görke, O., Pfeifer, P., Schubert, K., 2009. Kinetic study of ethanol reforming in a microreactor. Appl. Catal. A Gen. 360, 232–241.

Hsu, Y.-S., Wang, Y.-L., Ko, A.-N., 2009. Effect of Sulfation of Zirconia on Catalytic Performance in the Dehydration of Aliphatic Alcohols. J. Chinese Chem. Soc. 56, 314–322.

Hu, J. L., Wang, Y., Cao, C. S., Elliott, D. C., Stevens, D. J., White, J. F., 2005. Conversion of Biomass syngas to DME using a microchannel reactor. Ind. Eng. Chem. Res. 44, 1722–1727.

Jakobsson, K., Aittamaa, J., Alopaeus, V., 2014. Flowbat Software. `http://chemtech.aalto.fi/en/research/chemical_engineering/software/flowbat/`, accessed: 2014-12-04.

Kiwi-Minsker, L., Renken, A., 2005. Microstructured reactors for catalytic reactions. Catal. Today 110, 2–14.

Knözinger, H., Köhne, R., Apr. 1966. The dehydration of alcohols over alumina. The reaction scheme. J. Catal. 5 (2), 264–270.

Kolb, G., Hessel, V., 2004. Micro-structured reactors for gas phase reactions. Chem. Eng. J. 98, 1–38.

Krampera, F., Beránek, L., 1986. Kinetics of individual reactions in reaction network 1-butanol-di-(1-butyl) ether-butenes-water on alumina. Collect. Czechoslov. Chem. Commun. 51 (4), 774–785.

Lopes, J. a. P., Cardoso, S. S. S., Rodrigues, A. E., 2011. Criteria for kinetic and mass transfer control in a microchannel reactor with an isothermal first-order wall reaction. Chem. Eng. J. 176-177, 3–13.

Macho, V., Králik, M., Jurecekova, E., Hudec, J., Jurecek, L., Jun. 2001. Dehydration of C4 alkanols conjugated with a positional and skeletal isomerisation of the formed C4 alkenes. Appl. Catal. A Gen. 214 (2), 251–257.

Macias, O., Largo, J., Pesquera, C., Blanco, C., González, F., 2006. Characterization and catalytic properties of montmorillonite pillared with aluminum/lanthanum. Appl. Catal. A Gen. 314, 23–31.

Makarova, M., Sep. 1994. Dehydration of n-Butanol on Zeolite H-ZSM-5 and Amorphous Aluminosilicate: Detailed Mechanistic Study and the Effect of Pore Confinement. J. Catal. 149 (1), 36–51.

Mears, D. E., Oct. 1971. Tests for Transport Limitations in Experimental Catalytic Reactors. Ind. Eng. Chem. Process Des. Dev. 10 (4), 541–547.

Mostafa, M., Youssef, A., 1998. Structural and surface properties of SnO_2AlPO_4 catalysts in relation to their dehydration activities. Mater. Lett. 34, 405–410.

Pfeifer, P., 2012. Application of Catalysts to Metal Microreactor Systems, Chemical Kinetics. Dr Vivek Patel (Ed.). `http://www.intechopen.com/books/chemical-kinetics/application-of-catalysts-to-metal-microreactor-systems`.

Phung, T. K., Lagazzo, A., Rivero Crespo, M. A., Sánchez Escribano, V., Busca, G., 2014. A study of commercial transition aluminas and of their catalytic activity in the dehydration of ethanol. J. Catal. 311, 102–113.

Poling, B. E., Prausnitz, J. M., O'Connell, J. P., 2000. The Properties of Gases and Liquids, 5th Edition. McGraw-Hill Professional.

Reschetilowski, W. (Ed.), Aug. 2013. Microreactors in Preparative Chemistry. Wiley-VCH Verlag GmbH & Co. KGaA, Weinheim, Germany.

Rouge, A., Spoetzl, B., Gebauer, K., Schenk, R., Renken, A., 2001. Microchannel reactors for fast periodic operation: The catalytic dehydration of isopropanol. Chem. Eng. Sci. 56, 1419–1427.

Schmidt, S. A., Kumar, N., Reinsdorf, A., Eränen, K., Wärnå, J., Murzin, D. Y., Salmi, T., May 2013. Methyl chloride synthesis over Al_2O_3 catalyst coated microstructured reactor −− Thermodynamics, kinetics and mass transfer. Chem. Eng. Sci. 95, 232–245.

Spatenka, S., Fila, V., Bernauer, B., Fulem, J., Germani, G., Schuurman, Y., 2005. Modelling and simulation of microchannel catalytic WGS reactor for an automotive fuel processor. Chem. Ind. Chem. Eng. Q. 11 (3), 143–151.

Walter, S., Malmberg, S., Schmidt, B., Liauw, M. A., 2005. Mass transfer limitations in microchannel reactors. Catal. Today 110, 15–25.

Weisz, P., Prater, C., 1954. Interpretation of Measurements in Experimental Catalysis 6, 143–196.

West, R. M., Braden, D. J., Dumesic, J. A., 2009. Dehydration of butanol to butene over solid acid catalysts in high water environments. J. Catal. 262, 134–143.

Zapf, R., Becker-Willinger, C., Berresheim, K., Bolz, H., Gnaser, H., Hessel, V., Kolb, G., Pannwitt, A.-K., Ziogas, A., 2003. Detailed Characterization of Various Porous Alumina-Based Catalyst Coatings Within Microchannels and Their Testing for Methanol Steam Reforming. Chem. Eng. Res. Des. 81, 721–729.

Zhang, D., Al-Hajri, R., Barri, S. A. I., Chadwick, D., 2010. One-step dehydration and isomerisation of n-butanol to iso-butene over zeolite catalysts. Chem. Commun. 46, 4088–4090.